In Situ Voltammetric Sensor of Potentially Bioavailable Inorganic Mercury in Marine Aquatic Systems Based on Gel-Integrated Nanostructured Gold-Based Microelectrode Arrays

Mary-Lou Tercier-Waeber, Melina Abdou, Marianna Fighera, Justyna Kowal, Eric Bakker, Peter van Der Wal

In situ Voltammetric Sensor of Potentially Bioavailable Inorganic Mercury in Marine Aquatic Systems Based on a Gel-Integrated Nanostructured Gold-based Microelectrode Arrays

Mary-Lou Tercier-Waeber[a]*, Melina Abdou[a], Marianna Fighera[b], Justyna Kowal[a], Eric Bakker[a], Peter van der Wal[b].

[a]Department of Inorganic and Analytical Chemistry, University of Geneva, Geneva, Switzerland

[b]Ecole Polytechnique Fédérale de Lausanne (EPFL), Neuchâtel, Switzerland

**Corresponding author:Marie-Louise.Tercier@unige.ch*

Abstract

The development and field validation of newly designed nanostructured gold-plated gel-integrated microelectrode arrays (Au-GIME) applied to the direct *in situ* Square Wave Anodic Stripping Voltammetry (SWASV) quantification of the potentially bioavailable inorganic mercury (Hg(II)) species in coastal area are presented. The Au-GIME consists of arrays of 100 to 500 interconnected iridium (Ir)-based microdisks that are electroplated with renewable Au nanoparticles (AuNP) or Au nanofilaments (AuNF) and covered with an agarose gel. The gel protects the sensor surface from fouling and ensures that mass transport of analytes toward the sensor surface is by pure diffusion only and therefore independent of the ill-controlled convective conditions of the media. The responses of these sensors to direct SWASV measurements of inorganic Hg(II) at near-neutral pH were investigated first in synthetic media, then in UV irradiated marine samples. The analytical responses were found to be correlated to the number of interconnected microelectrodes and the morphology of the nanostructured Au deposits, and independent of the media composition for chloride concentration ≥ 0.2M (salinity S ≥ 13) and pH ranging from 7 to 8.5. The AuNF-GIMEs have detection and quantification limits at the low pM level, fulfilling the requirement of sentinel tools for real-time monitoring of the dynamic fraction of Hg(II) in coastal area. The AuNF-GIMEs were incorporated in an in-house advanced multi-channel sensing probe for remote *in situ* high-resolution trace metal monitoring. Field evaluation and validation were successfully performed as

part of a field study in the Arcachon Bay (France), from which environmental data are presented. This work marks the first time that an autonomous electrochemical sensing probe successfully measures Hg(II) and its hourly temporal variation *in situ* without chemical modification of the sample.

Keywords: Mercury; nanostructured gold; integrated antifouling membrane; on-chip microelectrode arrays; square wave anodic stripping voltammetry (SWASV); *in situ* monitoring; seawater.

The determination of mercury (Hg) in marine aquatic systems is challenging because of its occurrence at generally low-picomolar to sub-picomolar concentrations (Obrist et al., and references therein).[1] Even at these low concentrations, Hg is a contaminant of global concerns as it presents severe hazards to environmental resources and human health because of its bioaccumulation and biomagnification along the trophic chain.[2–4] Natural inputs of Hg to aquatic systems are from weathering of mercury-bearing rocks and degassing of the earth's crust. Anthropogenic sources include fossil fuel burning, discharges from industry (e.g. chlor-alkali electrolysis, electronics, paper pulp) and runoff of agrichemicals.[5,6] Major efforts on the reduction of Hg mining and production for industrial use have been made since the year 1970s. Today, the "by-product" sectors dominate anthropogenic emissions, especially fossil fuel combustion for power and heating accounting for nearly 50% of the total Hg atmospheric emissions.[7] Although projections forecast a rise in these emissions in the next decades,[8] global actions are taken to regulate further Hg emissions. In the year 2009 the Governing Council of United Nations Environmental Programme (UNEP) established a global, legacy binding agreement on Hg emissions. Despite these efforts to control anthropogenic emissions, numerous studies revealed no declines in Hg concentrations in marine aquatic systems and biota, especially in aquatic predators such as fishes and marine mammals.[9–11] This strongly suggests that while in the past centuries Hg contamination in many ecosystems mainly resulted from "external" anthropogenic Hg emissions, the contribution of "internal" processes that control the transformation and biological uptake of Hg introduced and stored into the system from past emissions is rising.[12]

Owing to the reactivity of Hg, its biogeochemical cycles are exceptionally sensitive to climatic (temperature, light, hydrology), geochemical (pH, complexing ligands, suspended particles), biological (feeding behavior of organisms) and ecological processes (organic carbon flux, microbial processes, food web structure and dynamics).[2,4,12] All dissolved Hg chemical forms in aquatic systems are linked through a pool of divalent inorganic mercury, Hg(II), by various physicochemical reactions and microbiological transformations such as bacterial and/or photo- methylation/demethylation and (photo-) oxidation/reduction reactions.[13,14] The development of analytical methods for routine monitoring of Hg(II) enabling *in situ* reagent-free pre-concentration followed by *in situ* quantification for routine monitoring of Hg(II) is therefore of prime interest (*e.g.* Lavoie et al.).[2]

Anodic Stripping Voltammetric (ASV) techniques are promising to achieve this goal. The instrumentation is inexpensive and can be miniaturized for *in situ* monitoring.[15,16] Gold (Au) is a most suitable electrode substrate if electrochemical Hg preconcentration is performed with an underpotential deposition (UPD) condition.[17] UPD results in a submonolayer to monolayer of stable adsorbed Hg whose structure is strongly dependent on the crystallographic plane of the gold.[18,19] At higher Hg concentrations, or after long deposition times, Hg becomes fully reduced to Hg(0) and starts to diffuse into the gold substrate. This causes progressive changes to the gold surface due to the formation of Hg-Au amalgam and ultimately results in the Hg peak potential shift and Hg peak current intensity lowering.[20] However, Hg levels in marine waters are sufficiently low for the deposition to occur in the UPD regime.

During the last four decades, several kinds of gold electrodes were reported for the stripping voltammetric or potentiometric quantification of mercury that include bulk,[21–23] film,[24,25] microwires [26,27] and microdisks.[28,29] Gold nanoparticles (AuNPs)-modified macroelectrodes for detection of Hg(II) have been the subject of more recent reports (*e.g.* Laffont et al. and references therein).[30] Indeed, nanomaterials have attractive physicochemical properties, including the enhanced diffusion of electroactive species, a high effective surface area, an improved selectivity, enhanced catalytic activity, thereby resulting in a higher signal-to-noise ratio.[31–33] Despite this tremendous attention, very few of the sensors reported have been successfully applied to the Hg(II) quantification at the low picomolar range ($\leq$ 20 pM) and without the need of sensor regeneration between measurements, in fresh and marine waters.[22,23,27,30] Moreover, these low detection limits were only reached in strongly acidic media ($0 \leq pH \leq 2$) and after sample collection and handling. The sample handling included the following pre-treatment steps: sample filtration and UV-digestion to eliminate

suspended particulate matters (SPM) and decompose the dissolved organic matter (DOM) that have tendency to adsorb on the sensor surface and give rise to fouling;[22,27,34] and sometimes medium exchange to minimize stripping of the gold itself by forming soluble chloro-gold complexes in the presence of high chloride concentration in acidic condition.[23] These sample pre-treatments are not desired because they increase analysis time and cost, and are a potential source of contaminations. Coupled with the need for stirring during the voltammetric preconcentration step, they also drastically increase the complexity of submersible devices, complicate their development and limit their use in autonomous long-term applications. More importantly, acidification of the sample will invariably modify the sample chemical equilibria, hindering the analysis of metal speciation.

We reported recently on the development of newly designed gel integrated nanostructured gold-based interconnected microelectrode arrays (Au-GIME) for direct arsenic (III) monitoring in aquatic systems.[35] These sensors consist of on-chip arrays of 100- to 500- interconnected Ir-based microdisks electrochemically plated with Au nanoparticles or Au nanofilaments and covered with an antifouling gel (AuNP-GIME and AuNF-GIME). They combine the attractive physicochemical properties of nanomaterials reported and the unique features of gel-integrated microelectrodes ($r \leq 10$ μm) for *in situ* environmental monitoring.[36,37] Briefly, microelectrodes exhibit hemispherical diffusion and a low ohmic drop that allows one to perform the trace metals preconcentration step of stripping voltammetric techniques in quiescent solution.[38,39] They exhibit better sensitivities and detection limits compared to macroelectrodes due to a significantly larger signal-to-noise (S/N) ratio resulting from their increased mass-transport and lower capacitance.[38] The gel displays anti-convective properties that ensures that mass transport of ions and small molecules within the gel is controlled by pure diffusion and remains independent of ill-controlled convective condition of the natural media.[40,41] The gel also ensures efficient exclusion of aquatic natural fouling materials with radius typically higher than 35 nm thus minimizing fouling problems.[42] Finally, the GIME signals recorded by SWASV at natural pH is selective due to the so-called dynamic metal species (Me_{dyn}). The Me_{dyn} are defined as the sum of the free metal ions and the sufficiently labile (high dissociation rate enabling to maintain the equilibrium during the preconcentration step) and mobile (high diffusion rate) inorganic and organic metal complexes/species of up to a few nanometers in size.[36,43,44] These metal species represent the metal fractions that are potentially available for bio-uptake by living organisms and especially microorganisms such as phytoplankton (the lower trophic level of the food chain).[45,46] Indeed, if diffusional mass transport in the external medium is the rate limiting step, metal complexes

contributing to the GIME signal are expected to contribute to metal bioavailability. If instead transport of metal across the biological membrane is the rate-limiting step, the biological response (*e.g.* internalization flux) can be directly related to the free metal ion in solution.[46] Therefore, GIME Me_{dyn} measurements are more appropriate than total dissolved metal concentration (Me_{diss}) for the assessment of metal ecotoxicological impact.

In this work we study and optimize the performance of these sensors for the direct detection of the dynamic fraction of the inorganic Hg(II) in marine aquatic systems using subtractive stripping voltammetry[47] including a halide desorption step.[27] The Hg(II) diffusion in the gel and the effect of chloride concentration and temperature on the voltammetric signal of Hg(II) are investigated. A first attempt is made to evaluate the Hg(II) complexes that might be sufficiently labile and mobile to be detected *in situ.* This is done by inter-comparing the experimental results with calculated mercury speciation using the chemical equilibrium metal speciation computer code model Visual MINTEQ (vMINTEQ; https://vminteq.lwr.kth.se). Finally, the Au-GIMEs with nanostructured Au layers that provide the best sensitivity are integrated into an in-house submersible multi-channel trace metal sensing probe (TracMetal)[15] and applied to hourly *in situ* autonomous $Hg(II)_{dyn}$ monitoring in the Arcachon Bay. The reliability and accuracy of the data recorded *in situ* with the direct sensing approach proposed here are evaluated and successfully validated by Gas Chromatography-Inductively Coupled Plasma-Mass Spectrometry (GC -ICP-MS) independent reference measurements.

Experimental section

Chemicals

All solutions were prepared using ultrapure deionised water (18.2 MΩ.cm; Milli-Q, Millipore®). Gold layer deposition was performed with tetrachloroauric acid ($HAuCl_4$, 99.99%; Aldrich®), and the gold renewal with potassium thiocyanate (KSCN; Fluka®). Boric acid (H_3BO_3) and dipotassium hydrogen phosphate (K_2HPO_4) for buffer preparation, hydrochloric acid (HCl), nitric acid (HNO_3), sodium chloride (NaCl), sodium nitrate ($NaNO_3$) and sodium hydroxide (NaOH) were of suprapur grade (Merck®). The antifouling membrane was prepared using high purity agarose (LGL agarose; Biofinex®). A stock solution of 5µM Hg were prepared by appropriate dilution of a 1g/L in HNO_3 atomic absorption standard solution (Aldrich®) and acidified to pH 2 with HCl. This stock solution was stored at 4°C before use. Standard solutions at lowest concentrations were prepared each day. The 50 to 200 mM borate synthetic buffer was prepared in the presence of 20 to 100 mM $NaNO_3$ and the pH was adjusted to 8 with 1M and 0.1 M NaOH. Standard reference fulvic acids from the Suwannee river (SRFA 2S101F, International Humic Substances Society) were used as model of low molecular (LM) dissolved organic matter (DOM). A stock solution of about 400 mg/L was prepared, filtered on 0.45 µm pore-size nitrocellulose membrane, and quantified by a Total Organic Carbon analyser (TOC-V CPH, Shimadzu®) to precisely determine the final fulvic acid concentration based on the carbon percentage in SRFA known as 52.34% (http://humic-substances.org/).

Microelectrode array geometries and preparation

On-chip Ir-based interconnected microdisk arrays with three different geometries were used as substrates for electrodeposition of the nanostructured gold microelectrodes. Details on their geometries and fabrication can be found elsewhere.[35,40] Briefly, the three geometries consisted of: 5 x 20; 10 x 19 and 10 x 50 iridium (Ir) microdisks of 5 µm in diameter and center-to-center interdistances of 150 to 190 µm. These devices were produced by thin-film technology on silicon wafer. 2000 Å thick silicon nitrite (Si_3N_4), Ir, and Si_3N_4 layers were deposited successfully (Fig. 1). The Si_3N_4 top layer was patterned by photolithography to define the Ir microdisk arrays, an Ir microcounter electrode (µCE) and the bonding pads. A SU-8 layer, patterned by photolithography around the Ir microdisk arrays, served as containment ring for the antifouling agarose gel membrane

and controlled its thickness. The thickness of the SU-8 layer was 300 µm for the 5x20 Ir microdisk arrays, and 150 µm for the 10x19 and 10x50 arrays. The individual devices were sliced, mounted on a printed circuit board, wire bonded and encapsulated with epoxy resin.

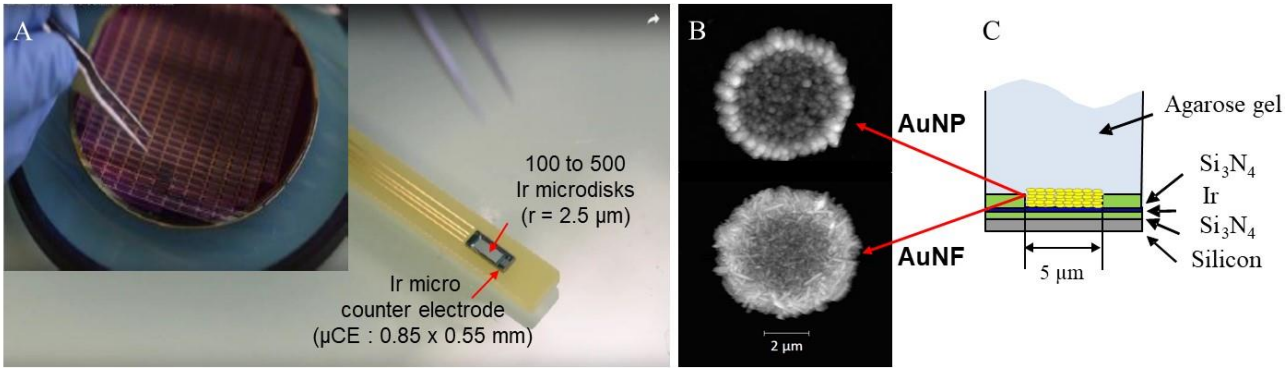

Figure 1: (A) Photos of the chip wafer and a single chip wire bounded and encapsulated on a PCB. (B) AFM images of the Au nanoparticle and Au nanofilament layers electrodeposited on one Ir microdisk. (C) Scheme of the various thin-layers and the gel.

The Au nanostructured layers were electrodeposited from a solution consisting of 1mM $KAuCl_4$ in 0.01M $HClO_4$, using the double-pulse chronoamperometric technique reported by Komsiyska and Staikov.[48] This method involves an instantaneous nucleation during a brief pulse step at potential E ≤ 0.65 V. During the second step, a slow diffusion controlled 3D growth of the Au nanoclusters formed occurs at potential ≥ 0.75V (step 2). For the first step, two different conditions were used to initiate the formation of the Au nanoclusters: 1) 0.5V for 2 s; and 2) 0.6V for 2s. The slow growth of the Au nanoclusters during the second step was performed for all sensors at 0.75V until reaching a defined reduction charge Q_{red} that corresponds to a theoretical average Au layer thickness ~500 nm per microdisk.[35] Gold nanoparticle (AuNP) and gold nanofilament (AuNF) layers were formed from the slow growth of the gold nanoclusters initiated at 0.5 and 0.6V, respectively (for details see: Tercier-Waeber et al.).[35] Once the Au nanostructured layers are deposited, they are stabilized in a 10^{-2}M HNO_3 solution by applying a constant potential of 0.7V for 5 min. At this stage, the Au-plated Ir-based microelectrode arrays can be kept in air in a dust-free environment. Coating of the sensor surface with the antifouling agarose gel was performed through simple dipping of the chip in a 1.5% LGL agarose solution heated at 80 °C. Further details on the gel characteristics and preparation are given elsewhere.[41] The nanostructured Au-plated gel-integrated microelectrode arrays (AuNP-GIME and AuNF-GIME; Fig. 1) were stored in 0.1M $NaNO_3$ pending and between experiments. Prior to

each new measurement cycle, the electroplated nanostructured gold must be activated. This was achieved in a 0.1M $NaNO_3$ and 10^{-3}M HNO_3 solution via three SWASV potential scanning cycles from -600 to +700 mV, after 1 min precleaning period at +700mV and a 2 min preconcentration step at -600mV (other SWASV parameters were as reported in the following section).

Instrumentation and experimental conditions

The electrochemical measurements in laboratory were performed using a PGSTAT101 Autolab potentiostat (Metrohm®) controlled by a laptop computer or an in-house potentiostat, and in-house acid-washed Plexiglas standard or flow-through cells based on three electrode systems. The working electrode was an AuNP-GIME or AuNF-GIME. The reference and counter electrodes, respectively, consisted of an in-house Ag/AgCl/3M gel KCl mini-electrode,[47] and the Ir µCE incorporated on each chip (Fig. 1A).[35] An in-house compact, fully integrated, submersible multi-channel trace metal sensing probe (TracMetal) was deployed for *in situ* $Hg(II)_{dyn}$ field monitoring.[15]

The subtractive SWASV protocol and conditions for $Hg(II)_{dyn}$ measurements consisted of the following continuous steps: (i) Precleaning step: E_{clean} = +700mV, t_{clean}= 60s; (ii) equilibration step: E_{eq} = -300mV, t_{eq} = 10s; (iii) Preconcentration step: $E_{preconc}$ = -300 mV, $t_{preconc}$ = 2 to 30 min; (iv) desorption step: E_{des} = -1100 mV, t_{des} = 30 to 60 s; (v) equilibration step: E_{eq} = -300mV, t_{eq} = 10s; (vi) Stripping step: initial potential (E_i) = -300 mV, final potential (E_f) = +700 mV, frequency (f) = 200 Hz, potential pulse amplitude (E_{sw}) = 25 mV, potential step height (E_s) = 8 mV. Before each measurement, a background scan was recorded using the same parameters but without preconcentration step. The background scan was subtracted from the analytical scan to obtain a corrected final scan.[47] The desorption step, added to the SWASV protocol, enables to avoid excessive adsorption of halide over time as demonstrated previously.[27,30] After this step, the potential was switched back to -300 mV for 10 s at the start of both background and stripping steps. During this equilibration time, the capacitive current should again decay exponentially. This procedure resulted in a much better match between background and baseline of the stripping voltammograms and allowed for a reliable subtraction of the background current. All measured solutions were deoxygenated through bubbling the solution with dinitrogen (N_2) during 10 min before measurements

and keeping a N_2 flow at the surface of solution during the measurements. During field application, an in-house on-line oxygen removal system was used.[49]

The accuracy of the analytical response of the nanostructured Au-GIME was evaluated by analysis of a European Certified Reference Material (CRM) consisting of coastal seawater acidified at pH 2 and spiked with Hg(II) (ERM®-CA400, EU Joint Research Center; Hg(II) certified value = 83.7*5* ± 5.4*8* pM), after 20% dilution in a 0.1 M boric acid buffer and adjusting the pH at 8. The 5x20, 10x19 and 10x50 AuNP-GIME and AuNF-GIME arrays provided recoveries within the range of 97 to 105% using respectively 20 and 10 min t_{prec} and the precision expressed as % of the relative standard deviation (%RSD; n = 3) was ≤ 10%.

The total dissolved Hg(II) concentrations in the 0.2 μm fraction ($Hg(II)_{diss}$) and dissolved organic carbon (DOC) in collected samples were determined by respectively Gas Chromatography-Inductively Coupled Plasma-Mass Spectrometry, GC-ICP-MS, (X7 Series, Thermo®) applying the Isotope Dilution (ID) method as published elsewhere,[50] and with an automated analyzer (TOC-L, Shimadzu®) as detailed by Sharp et al.[51]

Field tests area, in situ measurements and water sampling for ancillary measurements

Field application and evaluation were performed on 15-16 May 2017 at the Comprian site (44°40.823'N, 1°05.902'W) in the Arcachon Bay. Located in southwest France, ~100 km to the south of the Gironde Estuary mouth, the Arcachon Bay is a meso-tidal lagoon. This lagoon is of major socio-economic interest since it represents an important breeding ecosystem for regional seafood production, especially oysters. The sampling site, Comprian, is located in a main current channel of the bay and is characterized by the influence of the inputs from the Leyre River, several cities surrounding the site (~90,000 inhabitants), and Atlantic Ocean seawater. The TracMetal,[15] incorporating a 190-AuNF-GIME, was coupled to an Idronaut® OS316 multiparameter probe. This integrated sensing system was deployed at 2.5m depth from the R/V Planula IV (TGIR FOF).

Salinity and turbidity were recorded *in situ* every 15 min by the multiparameter probe jointly deployed with the TracMetal. Hourly AuNF-GIME SWASV measurements of the dynamic fraction of Hg(II) ($Hg(II)_{dyn}$) were performed during a 24h cycle. The 190-AuNF-GIME calibrations for Hg(II) in the range of 2 to 8 nM ($t_{preconc}$ = 10 min) were done before and after the temporal profile

measurements in, respectively, pH 8 (0.02 M borate buffer) 0.3 M NaCl suprapur as external calibration in the field laboratory and a collected seawater sample as on-board internal calibration. Normalized calibration slopes were, respectively, (4.2 ± 0.03) and (3.9 ± 0.03) nA/nM min. The temporal $Hg(II)_{dyn}$ concentrations were determined using the average values of the external and internal normalized calibration slopes, after correction of the influence of temperature on the Hg SWASV signals recorded *in situ* using the factor determined in laboratory (see section "Correction factor for temperature effect"). Vertical error bars in Fig. 6 represent the average RSD of 13% determined from triplicate on-board measurements in a collected sample before and after the 24 h measurement cycle.

Sample collection was performed for ancillary measurements of total dissolved Hg(II) ($Hg(II)_{diss}$) by GC-ICP-MS and DOC. It was achieved using an in-house 12V battery-powered peristaltic pump and an acid-washed Teflon tubing affixed to the titanium protective cage of the TracMetal. Samples were placed into acid-cleaned polypropylene (PP) bottles that had previously been rinsed three times with the sub-surface water from the site. For the quantification of $Hg(II)_{diss}$, the samples were immediately filtered on-site through 0.2 µm Minisart® cellulose acetate filters. Filtrates were placed into acid-cleaned Teflon FEP bottles (Nalgene®), acidified with HCl (1/1000 v/v; J.T. Baker Instra® 36.5 – 38 %), and then stored at 4 °C in the dark pending analysis. Aliquots for DOC quantification were filtered through pre-combusted (500 °C, 4 h) glass-fiber filters (0.7 µm, Whatman® GF/F) using a pre-washed (RBS detergent, carefully rinsed with ultrapure deionised Milli-Q® water) and pre-combusted glass syringe. Filtrates were placed into pre-washed and pre-combusted glass bottles and acidified with HCl (3/1000 v/v; J.T. Baker Instra® 36.5 – 38 %). The bottles were covered by aluminium foil, and then kept in the dark at 4 °C until their analysis.

Results and discussion

Influence of chloride concentration and pH

Estuaries and coastal aquatic systems are characterized by pH ranging from 7.5 to 8.5 and Cl^- concentrations ranging from 10^{-4} to 0.6 M. We therefore first investigated the influence of these two parameters on the response of the Au-GIME for direct quantification of inorganic Hg(II) by SWASV.

The influence of chloride concentration was studied at pH 8 (borate buffer) in synthetic solutions of 20 nM Hg(II) containing $NaNO_3$ and NaCl to vary the chloride concentration while keeping the ionic strength fixed at 0.5M (Fig. 2) to 1M (see section "Evaluation of the dynamic Hg(II) species"). The stripping peak current intensity was found to dramatically increase for Cl^- concentrations of 10^{-4} to 0.1 M (Fig. 2A) prior to reaching a plateau for concentrations ≥ 0.2M (see section "Evaluation of the dynamic Hg(II) species", Fig. 5C). This suggests the presence of electrochemically inert Hg chemical species for Cl^-concentrations < 0.2M at near-neutral pH (see section "Evaluation of the dynamic Hg(II) species" for more detail). The peak potential shifted negatively with increasing concentration of Hg chloro-complexes (Fig. 2A, B). A linear relationship was observed between the peak potential and -log (Cl^-) with slopes of 59.1 mV and 58.3 mV (Fig. 2B) using, respectively, a 190 AuNF-GIME and a 500-AuNP-GIME. These results are consistent with a Nernstian contribution of chloride during the Hg(0) reoxidation (stripping step) via the formation of intermediate $Hg(Cl)_2$ complexes suggested previously by Moretto et *al.*[52] and Belevantsev et *al.*[53]

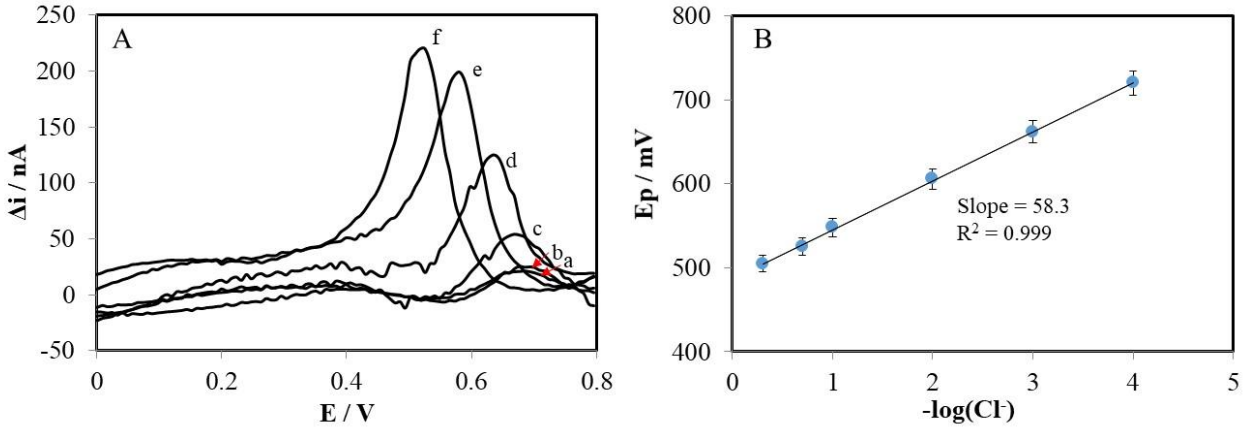

Figure 2: (A) Hg(II) SWASV voltammograms for increasing concentrations of Cl^- : a) 0, b) 10^{-4}M, c) 10^{-3}M, d) 10^{-2}M, e) 0.1M, f) 0.5M. (B) Shift in peak potential Ep as a function of -log (Cl^-); Cl^- concentrations ranging from 10^{-4}M to 0.5M. 20 nM Hg(II); 500-AuNP-GIME; $t_{prec.}$: 5 min.

The influence of pH was investigated in 0.2 M NaCl solution buffered to pH 7 to 8.5 using phosphate or borate buffers. Relative standard deviation of less than 5% were observed for the SWASV signals of 10 nM Hg(II) recorded with a 190-AuNF-GIME. For all subsequent measurements in synthetic solutions, 0.2M NaCl at pH 8 with borate buffer was used as electrolyte.

Kinetics of Hg(II) diffusion through the agarose gel

To minimize fouling problem and interference of ill-controlled convective conditions, the LGL agarose gel layer was selected to be thicker (300 µm for the 100-Au-GIME and 150 µm for the 190- and 500- Au-GIME) than the microelectrode diffusion layer thickness. This means that voltammetric measurements are performed inside the gel after its equilibration with the sample and therefore influenced by the gel properties. A knowledge of the diffusion kinetics of analyte in the gel allows one to determine the required equilibration time for a given gel thickness and assess whether the gel is chemically inert toward the analyte as previously published.[34,40,41] For this, a Au-GIME was placed in a blank electrolyte (pH 8 borate buffered 0.2M NaCl), and three replicate measurements performed. 100 nM Hg(II) was then added to the electrolyte and SWASV measurements were performed every 40s until the Hg(II) peak current reached a plateau. The solution was then rapidly substituted by a fresh blank electrolyte, and the diffusional loss of mercury was monitored by SWASV measurements as before. Typical profiles obtained for Hg(II) diffusion towards and away from the sensor surface are shown in Fig. 3.

The time needed for the equilibration of the gel was assessed from the value of t_{95}, i.e. the time required for the Hg(II) concentration at the surface of the electrode to be 95% of the concentration in bulk solution ($\Delta i/\Delta i_{max}$ = 95%). This time was found as 4.3 ± 0.5 min and 2.9 ± 0.4 min for gel thicknesses of, respectively, 300 (100-Au-GIME) and 150 µm (190- and 500-AuGIME). These times were similar to those determined from the value of t_5 for the measurements of Hg(II) diffusion out of the gel (Fig. 3), suggesting that the gel is chemical inert to Hg(II). To ensure that the gel is equilibrated with the bulk solution prior to each measurement, the gel equilibration time was set to 5 min in the SWASV protocol (see section “Instrumentation and experimental conditions”).

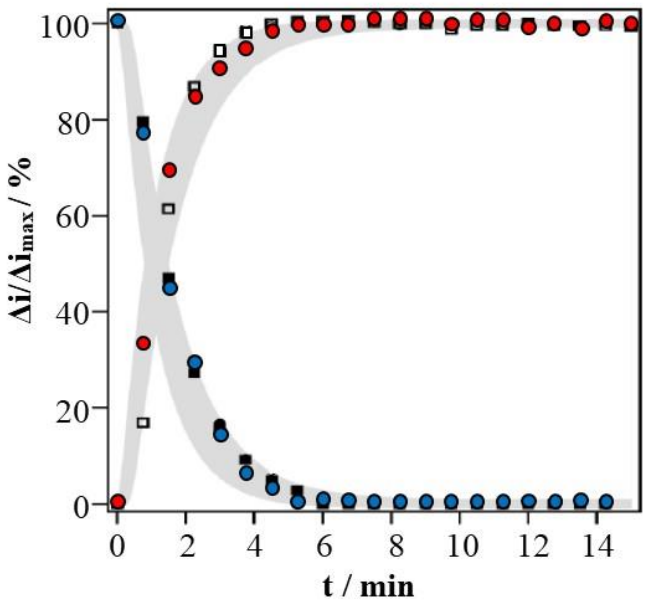

Figure 3: Experimental (symbols) and theoretical (grey area) Hg(II) diffusion profiles in 300 ± 25 µm thick 1.5% LGL agarose membrane, toward (red circle, open square) and from (blue circle, black square) the microlectrode array surface. 100-AuNP-GIME. SWASV precleaning and preconcentration times were set at 10 and 20 s respectively.

The diffusion coefficients of Hg(II) in the gel were determined with eq 1,[54] based on calculation of free diffusion of a substance through a membrane of thickness l under the limiting condition of $(0.2\ C_{sol} + 0.8\ Cm) \leq C \leq (0.9\ C_{sol} + 0.1\ C_m)$:[41]

$$\ln\left[\frac{C^* - C(t)}{C^* - C(0)}\right] = 0.2306 - 2.452\,\frac{D.t_{eq}}{l^2} \qquad (1)$$

where: C^* is the bulk concentration in solution (constant), C(0) the initial uniform concentration in the gel, C(t) the concentration at the microelectrode surface (i.e. x = 0) at time t, D the diffusion coefficient, t_{eq} the equilibration time and l the thickness of the gel.

The diffusion coefficients were independent of the 1.5% agarose gel thickness, confirming the inertness of the LGL agarose to Hg(II) species. The average diffusion coefficient for Hg(II) in the agarose gel, calculated from the diffusion profiles, was determined as $(4.3 \pm 0.3) \times 10^{-6}$ cm^2 s^{-1} in the range of the investigated gel thicknesses (150 or 300 µm).

A finite difference numerical simulation was performed to support results from the experimental data. Accordingly, the Fick's second law was applied (eq 2) to simulate the mass transport in a homogeneous phase for a one-dimensional diffusion problem:

$$c_n(t + \Delta t) = c_n(t) + \{c_{n-1}(t) - 2c_n(t) + c_{n+1}(t)\}\frac{D.\Delta t}{\delta^2} \quad (2)$$

where: c is the concentration, D the Hg(II) diffusion coefficient in the gel, t the time, Δt the time increment, δ the thickness of each element and n the position. Values for Δt and δ were chosen as respectively 0.01 s and 25 µm.

The diffusion coefficient was adjusted until reaching a good agreement between simulated (Fig. 3, grey area) and observed behaviour (Fig. 3, symbols). A theoretical diffusion coefficient of 4.1 x 10^{-6} $cm^2.s^{-1}$ for Hg(II) in the gel was then determined through calculation, allowing for an uncertainty in the gel layer thickness of ±25 µm. The numerical simulation confirmed the values from eq 1 with a difference of 7%. When the diffusion coefficient is compared to the one reported by Henry [55] as 8.4 x 10^{-6} $cm^2.s^{-1}$, the ratio $D_{gel}/D_{free\ sol}$ is 0.51 (from eq 1) and 0.49 (from simulation). Tercier et al.,[41] Belmont-Hébert et al.,[40] and Touilloux et al.[34] demonstrated that the diffusion coefficient in 1.5% LGL agarose decreased by about half for cation and neutral oxyanion analysis owing the gel physical properties (mesh size, fiber diameter, macroreticulate networks) influencing ion mobility. The results suggest that the gel is behaving the same for negatively charged inorganic metal complexes.

Temperature effect correction

The temperature is known to influence the rate of diffusion. In aquatic systems, temperatures may vary between 25 to 5°C according to the depth, therefore requiring a temperature correction of the voltammetric signal recorded *in situ*.[40,57] For this purpose, a procedure based on Arrhenius' law, introduced and aopplied by us for other trace metals,[34,40] were used to determine an experimental correction factor for temperature effect on the voltammetric Hg signal. Briefly, according to Arrhenius' law (eqn (3)), the diffusion coefficient D is ideally expected to be proportional to $\exp(E_a/RT)$. Since the peak current intensity at microelectrodes during the preconcentration step is directly proportional to D (eq 4),[39] a linear relationship can be expected between ln(i) and 1/T (eq 5).

$$D = D_0 . e^{\frac{-E_a}{RT}} \quad (3)$$

$$\rightarrow i \propto D \rightarrow i = i_0 . e^{\frac{-\Delta G}{RT}} \quad (4)\ (5)$$

where: D is the diffusion coefficient, D_0 the maximum diffusion coefficient (at infinite temperature), E_a the activation energy, ΔG the free enthalpy, T the temperature and R the gas constant. ΔG is similar to E_a for reversible systems. For quasi-reversible and irreversible systems, charge transfer kinetics becomes the limiting factor and ΔG is significantly higher than E_a.

Eq (5) suggests that the slope $\Delta G/R$, i.e. the correction factor for temperature effect, can be determined experimentally and applied later to correct for the temperature influence on the SWASV current monitored *in situ* using eq (6):

$$i\,(T_{cal}) = i\,(T_{in\ situ}).\exp\left(\frac{\Delta G}{R}\left(\frac{1}{T_{cal}} - \frac{1}{T_{in\ situ}}\right)\right) \quad (6)$$

where $T_{in\ situ}$ is the sample temperature measured *in situ*, T_{cal} is the temperature during the calibration, $i\,(T_{in\ situ})$ is the SWASV current measured *in situ* at $T_{in\ situ}$ and $i\,(T_{cal})$ is the SWASV current which should be measured at T_{cal}.

The experiment was done with a 10 nM Hg(II) solution and without a gel layer on the electrode array, assuming that the correction factor should be similar to the one obtained with gel coating.[40] A linear T ramp was applied from 25°C to 5°C and 5°C to 25°C with a step of 5°C and repeated three times. We indeed observed a linear relationship between ln(i) and 1/T. The temperature effect correction factor, $\Delta G/R$, determined from the slope of the replicate experimental curves was found to be -3163 ± 47 K. A comparison is possible between this experimental value and the theoretical value for a reversible system, E_a/R = - 2555 K, provided by the Stokes-Einstein equation for linearity between ln (D) and 1/T.[57] The experimental Hg slope is just slightly higher than predicted for diffusion-controlled systems. This shows that the peak current behaves as a reversible system for the fast SWASV conditions applied here (scan rate of 1.6 V/s).

Reliability and sensitivity of the Au-GIME

The three on-chip arrays exhibit inter-distance between the microelectrodes sufficient to prevent overlapping of the diffusion layers and are covered by an LGL agarose gel. It was demonstrated that during the SWASV preconcentration step at GIME, the mass transport of metal ions toward the

surface of the integrated microelectrodes is controlled by pure diffusion thanks to the non-convective properties of the gel.[40,41] Under these conditions, the current intensity monitored for the re-oxidation of the metals during the stripping ramp should be proportional to the metal concentration in solution as well as the preconcentration time. The analytical performance as a function of the number of microelectrodes and the morphology of the Au nanostructured layers for Hg(II) quantification were studied through Hg(II) calibrations in the range of 1 to 10 nM. Moreover, the Hg(II) peak current intensity was measured as a function of preconcentration time at a constant Hg(II) concentration. This was first performed in synthetic solution (pH 8 borate buffered 0.2M NaCl) and subsequently in pH 8 (borate buffer) UV irradiated seawater samples (Table 1). Additionally, the measurement of the background allows one to evaluate the absence of Hg(II) signals on the background voltammogramms for the explored Hg(II) levels and preconcentration times. This may serve to assess whether complete stripping of Hg from the nanostructured gold microelectrode array has been achieved by the end of each stripping scan.

We also investigated the potential interference from co-deposited Cu(II) that might result in an overlap with the Hg(II) peak and/or a change in the electrode surface that might impact UPD Hg deposition. For this, data from SWASV voltammograms for laboratory total dissolved Hg(II) and Cu(II) in synthetic solution (pH 8 borate buffered 0.2 M NaCl) and UV irradiated filtered seawater, and for *in situ* measurements of the Hg(II) and Cu(II) dynamic species ($Hg(II)_{dyn}$, $Cu(II)_{dyn}$) in Arcachon Bay, were used.

Examples of SWASV stripping, background, and resulting subtractive voltammograms measured at a 100-AuNP-GIME in synthetic solution in absence and presence of Cu(II) are shown in Fig. 4 A and B. The background signals matched the baseline of the stripping voltammograms, allowing for a reliable subtraction of the background current. The Hg(II) and Cu(II) peaks were well resolved and the Hg(II) reoxidation peak currents were similar in the absence or presence of Cu(II), *e.g.* 67.8 ± 2.1 and 70.3 ± 3.2 nA for the conditions in Fig. 4 A and B, respectively. This suggests an absence of direct copper interference and that the Au-GIME has promising ability for the simultaneous measurements of Hg(II) and Cu(II), despite the need for more characterization for various Cu(II) to Hg(II) concentration ratios (see below). Measurements at a 190-AuNF-GIME performed in pH 8 UV irradiated seawater samples gave a larger background current, but this parasitic signal was again efficiently subtracted with the SWASV protocol used (Fig. 4 C). A shift of ~30 mV toward higher

potentials was observed for Cu(II). Nevertheless, this copper peak shift did not negatively impact the resolution of the Hg(II) peak in a significant way. This is confirmed by the SWASV voltammogram recorded *in situ* in the Arcachon Bay (Fig. 4D) where the concentration of $Cu(II)_{dyn}$ was 0.4 nM, i.e. ~ 30 times higher than $Hg(II)_{dyn}$ levels (see Tercier-Waeber et al. for more detail).[15] However, a 20 min co-deposition time of 0.4 nM Cu may result in a coverage of up to 8 monolayers. Such a multilayer Cu coverage at the nanostructured gold might impact the UPD of Hg(II). This was evaluated and discussed more in detail in the sub-section "Field application and evaluation".

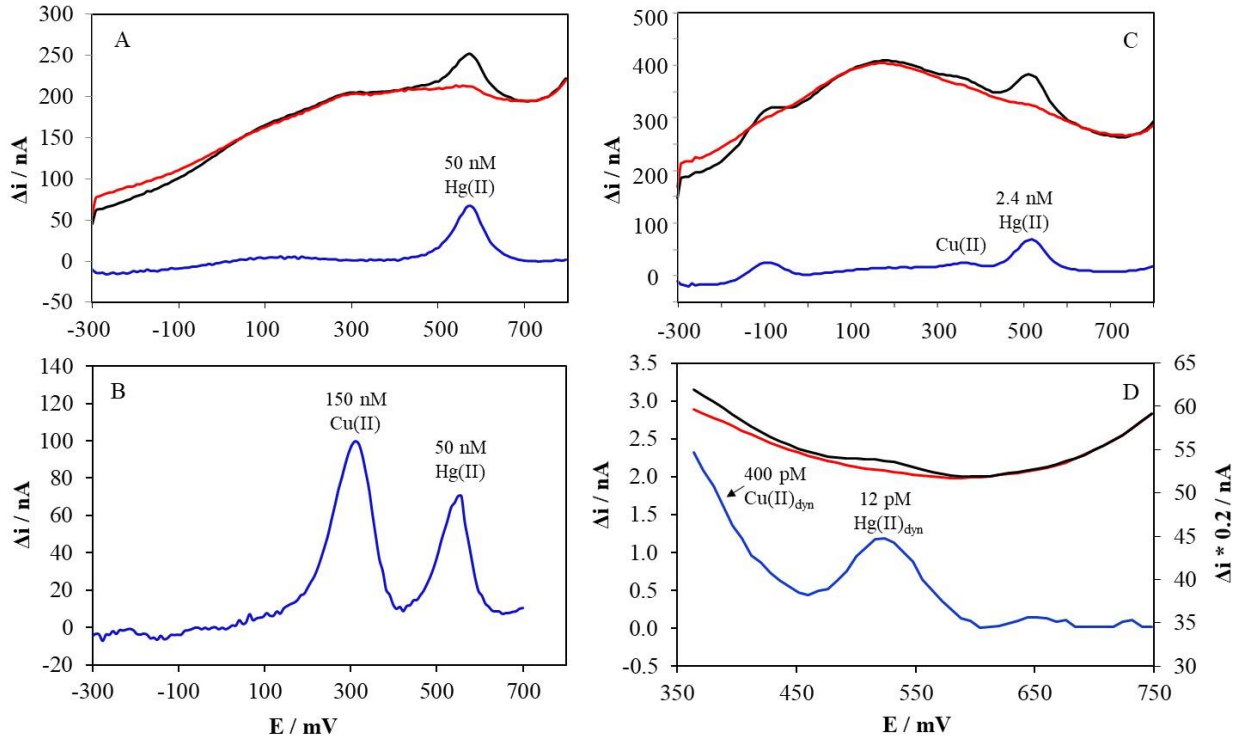

Figure 4: (A) SWASV stripping (black), background (red) and subtractive (blue) voltammograms recorded with a 5x20-AuNP-GIME for 50 nM Hg(II) in pH 8 (borate buffer) 0.2 M NaCl ($t_{preconc.}$= 2 min); (B) Same as (A) after addition of 150 nM Cu(II). (C - D) SWASV stripping (black), background (red) and subtractive (blue) voltammograms recorded with a 10x19-AuNF-GIME in (C) UV irradiated seawater sample after addition of 2.5 nM Hg(II) ($t_{preconc.}$= 6 min); and (D) *in situ* in the Arcachon Bay ($t_{preconc}$ = 20 min). Each background scan was recorded in analogy to the stripping scan but without preconcentration (see experimental section for detail).

Hg(II) signals were not observed in the background voltammogramms of the *in situ* hourly measurements performed during the 24-h cycle in the Arcachon Bay (see Fig. 4D), suggesting an

efficient stripping of Hg from the nanostructured Au microelectrodes by the end of each stripping scan. For Hg(II) concentrations ranging for 1 to 50 nM and $t_{preconc} \leq 6$min (*e.g.* Fig. 4 A and C), Hg(II) signals appeared on the background voltammogramms. Here, however, the ratio of the background to the stripping Hg(II) signals were similar to the ratio of the equilibrium to the preconcentration times. This suggests that the observed signals were mainly caused by Hg(II) preconcentrated during the 10s equilibration step and not by incomplete Hg stripping. Hg(II) preconcentration during the equilibration step does not influence the subtractive SWASV Hg(II) peak current as this step is performed before both the stripping and background scans.

The calibration curves and the currents as a function of preconcentration time gave good linearity and reproducibility (Table 1). Moreover, for a given geometry, the associated normalized slopes were similar, as expected in absence of the overlapping of the diffusion layers of the microelectrode arrays. These results confirm that during the preconcentration step, the flux of analyte in the gel occurs by diffusional mass transport thanks to the non-convective properties of the gel[36,40,41] and by radial steady state at the electrodes surface owing to their micrometric size. This means that (i) the preconcentration step can be done in quiescent solution, which greatly improves the reliability of the measurements;[40] and (ii) normalized calibration slopes obtained from laboratory measurements at a short preconcentration time can be applied to adjust for various preconcentration times. This is of major importance in view of any *in situ* application of these sensors. Moreover, the similar normalized slopes for a given geometry obtained from the calibration curves and the currents as a function of preconcentration time also support that the Hg chloro-complexes are fully labile. The dissociation rate is sufficiently rapid to maintain equilibrium with the free metal ions during a preconcentration time of at least 30 min. The good agreement between the normalized slopes recorded in synthetic and UV irradiated seawater confirms the negligible influence of Cl^- ranging from 0.2 to 0.6 M on the nanostructured Au-GIME SWASV quantification of $Hg(II)_{dyn}$ at near-neutral pH. This is supported by a precision (%RSD of the average normalized slopes) of ≤ 11% and ≤ 7% for the nanostructured AuNP-GIME and AuNF-GIME, respectively (Table 1).

Table 1: Normalized slopes (NS), expressed in nA/nM min, determined from calibration curves and measurements of $\Delta i = f(t_{preconc})$ for the three geometries of (A) AuNP-GIME and (B) AuNF-GIME. Hg(II) ranging from 2 to 10 nM and a $t_{preconc}$ of 10 min were used for the calibrations. The $\Delta i = f(t_{preconc})$ curves were recorded in presence of 2 or 10 nM Hg(II) using $t_{preconc}$ in a range of 5 to 30 min. All solutions were diluted by 20 % with 0.2 M borate buffer to keep the pH at 8. No µ-el. = number of microelectrodes per chip; SG = sensitivity gain as a function of: (A) and (B) the number of microelectrodes (SG No µ-el.; and (B) the Au layer morphologies (SG AuNF vs AuNP). *Precision: %RSD of the average value of the normalized slopes obtained from Hg(II) measurements in the synthetic solution and UV irradiated natural sample (n = 9 to 15).

A) **AuNP-GIME**

	NS : calibration (n = 3 to 5)			**NS: i = f ($t_{preconc.}$) (n = 3 to 5)**		
No µ-el.	**100**	**190**	**500**	**100**	**190**	**500**
0.2 M NaCl	0.51 ±0.02*2*	1.08±0.06*7*	1.98±0.18*3*	0.58±0.03*7*	1.10±0.05*4*	2.15±0.21*4*
UV Seawater	0.55±0.04*4*	1.12±0.08*7*	2.06±0.145	0.56±0.10*5*	1.12±0.09*4*	2.13±0.11*2*
Average *Precision	**0.53±0.03*3*** (6.2)	**1.10±0.071** (6.5)	**2.02±0.162** (8.1)	**0.57±0.06*1*** (10.7)	**1.11±0.07*4*** (6.7)	**2.14±0.15*2*** (7.1)
SG No µ-el.	1	2.0	3.8	1	1.9	3.7

B) **AuNF-GIME**

	NS calibration (n = 3 to 5)			**NS i = f ($t_{preconc.}$) (n = 3 to 5)**		
No µ-el.	**100**	**190**	**500**	**100**	**190**	**500**
0.2 M NaCl	1.98 ±0.13*0*	4.48±0.45*0*	8.10±0.24*7*	2.14±0.09*7*	4.30±0.08*7*	8.18±0.21*0*
UV Seawater	2.09±0.11*3*	4.06±0.34*0*	7.92±0.28*1*	2.16±0.14*4*	4.12±0.26*8*	8.23±0.27*2*
Average *Precision	**2.03±0.12*8*** (6.3)	**4.20±0.27*7*** (6.6)	**8.00±0.23*6*** (3.0)	**2.15±0.13*5*** (6.3)	**4.20±0.21*1*** (5.02)	**8.20±0.39*6*** (4.8)
SG No. µ-el.	1	2.1	3.9	1	1.9	3.8
SG AuNF vs AuNP	3.8	3.8	3.9	3.8	3.8	3.8

The influence of the number of microelectrodes and of the morphology of the nanostructured Au layer on the sensor sensitivity were assessed through the comparison of the average normalized slopes of the calibration curves and the measurements for various preconcentration times (Table 1). An increasing sensitivity of typically 1.9 (proportional to the microelectrode number ratio) and 3.7 to 3.8 (less that the number of the microelectrode ratio) were obtained for the 190- and 500- interconnected

arrays in comparison to the 100 interconnected microelectrodes. These results are in good agreement with those observed for As(III) quantification using these sensors.[35] The non-proportionality obtained between the 100- and 500- interconnected microsensors might be linked to an increase of impedance with the increase of on-chip sensor surface area: the area of the chip containing 500 microelectrodes is 1.8 times larger than the chips for 100- and 190- microelectrodes. Impedance measurements are required to verify this hypothesis, but this was out of the scope of this paper. The sensitivities of AuNF-GIME were typically four times higher than those of the AuNP-GIME, independently of the number of microelectrodes (Table 1). A similar difference in sensitivities between the two nanostructured Au morphologies was observed for As(III) detection.[35] Therefore, the results of Table 1 support the hypothesis of a higher signal to noise ratio due to a larger electrochemically active area for the AuNF-GIME, and/or a quicker electron charge transfer at the AuNF microelectrodes.

The limits of detection (LD) and quantification (LQ), calculated on the basis of respectively 3.3x and 10x the standard deviation of the regression lines divided by the slopes, are shown in Table 2.

Table 2: Analytical performances of the three geometries of the AuNP-GIME and AuNF-GIME for direct SWASV Hg(II) analysis in seawaters. LD-10, LQ-10 and LD-30, LQ-30: limits of detection and quantification using a preconcentration time of 10 and 30 min, respectively.

	LD-10 / pM	**LD-30 / pM**	**LQ-10/ pM**	**LQ-30 / pM**
AuNP-GIME				
5 x 20	100	28	300	100
10 x 19	40	15	130	50
10 x 50	12	5	40	15
AuNF-GIME				
5 x 20	20	6	60	20
10 x 19	8	2	24	6
10 x 50	3	1	9	3

The sensor performances indicate that all the developed sensors, especially the 10x19- and 10x50-interconnected AuNF-GIME, are promising tools for the direct detection and measurement of inorganic Hg(II) at low pM concentrations in coastal areas (see section 3.6).

Evaluation of the dynamic Hg(II) species

As demonstrated previously for copper, lead, cadmium, zinc,[58,59] manganese[60] and arsenic,[61] GIME sensor interrogated by SWASV are selective to the so-called dynamic fraction of trace metals. This represents the fraction of metals potentially bioavailable to aquatic organisms and especially phytoplankton, and thus it is relevant in terms of (eco)toxicity. Knowing the Hg(II) chemical forms that will be quantified using the nanostructured Au-GIME developed here is therefore of prime interest.

In seawater inorganic Hg(II) speciation is thought to be mainly controlled by complexation with chloride, bromide and dissolved organic matter (DOM). Recent studies demonstrated that DOM in coastal water is dominated (≥ 75%) by low molecular weight (MW≤ 2kDa) hydrophilic fulvic-like organic matter.[62,63] The size of these predominant DOM, based on their MW, can be estimated to be a few nanometers. Therefore, Hg(II) complexes with these small DOM may diffuse through the gel and contribute to the observed $Hg(II)_{dyn}$ fraction.

As a first attempt in the assessment of the dynamic Hg(II) chemical species, the vMINTEQ computer code model was used to predict the main Hg chemical forms and their proportion i) as a function of the chloride concentration in synthetic solution at pH 8 and ionic strength of 0.5M (Fig. 5A); and ii) in seawater in absence and presence of dissolved organic matter (DOM; Fig. 5B). These values were then compared with the Δi Hg(II)/Δimax Hg(II) ratios recorded with the Au-GIME under the same conditions in controlled solutions (Fig. 5 C and D). Standard reference Suwannee River fulvic acid (SRFA) were chosen to mimic the low MW DOM (i.e. FA) found in coastal areas (Fig. 5 B and C). SFRA in concentrations ranging from 1 to 6 mg/L were added to aliquots of an UV irradiated water sample and stored for 18 to 20h for equilibration of the SFRA with the seawater compounds. Measurements were performed 15 min after the addition of 5 nM Hg(II) to the samples spiked with increasing concentration of SFRA. The SRFA are the most hydrophilic of the standard humic-like substances and therefore the one the least likely to aggregate under environmentally coastal relevant conditions of pH and ionic strength.[64] They have a size of 1.5 to 2.5 nm[64] and their diffusional properties in water and the LGL agarose were characterized for the relevant interpretation of trace metal chemical speciation from GIME data.[67]

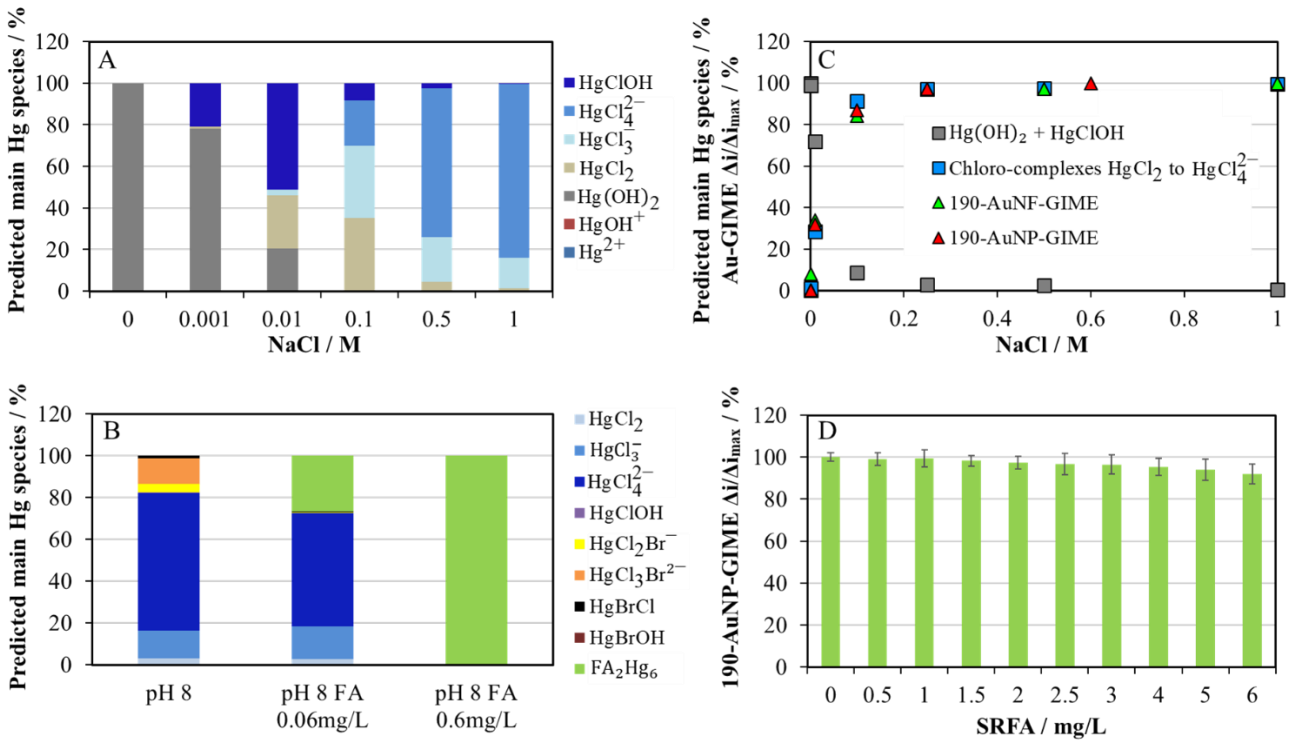

Figure 5: Hg speciation predicted by vMINTEQ in: (A) pH 8 $NaNO_3$ and increasing concentrations of Cl^-; (B) UV irradiated seawater in absence or presence of low MW DOM (FA). Nanostructured Au-GIME SWASV $\Delta i / \Delta i_{max}$ Hg(II) ratios measured in (C) pH 8 $NaNO_3$ and increasing concentration of Cl^-; and (D) in pH 8 UV irradiated seawater in absence and presence of increasing concentration of fulvic acid (SRFA). (C): $NaNO_3$ concentration was adjusted to maintain the ionic strength at 0.6M or 1M for measurements performed with the 190- AuNP-GIME and AuNF-GIME, respectively. Hg(II) concentrations: 2 to 10 nM; $t_{preconc}$: 5 to 10 min.

Fig. 5A shows that in synthetic solution at pH 8 in the absence of chloride, Hg(II) is present mainly in the hydroxide form as $Hg(OH)_2$. When the chloride concentration increases, chloride competes with hydroxide for Hg(II) complexation. For $Cl^- \geq 0.1M$, the proportion of the chloro-complexes ($HgCl_2$, $HgCl_3^-$, $HgCl_4^{2-}$) increases in order of their complex formation constants (β_{2-4} = 13.22, 14.10, 15.10; Lindgren et al.).[66] The increase in the ratios $\Delta i/\Delta i_{max}$ determined from the AuNF-GIME and AuNP-GIME measurements as a function of Cl^- concentration follows the increase of the chloro-complexes proportion predicted by vMINTEQ (Fig. 5C). These results suggest that all the Hg chloro-complexes ($HgCl_2$, $HgCl_3^-$,$HgCl_4^-$) contribute to the recorded Me_{dyn} fraction, while the Hg

hydroxo- and hydroxo-chloro-complexes ($Hg(OH)_2$, HgClOH) are not electrochemically accessible (Fig. 5C). In seawater in the absence of DOM, Hg chloro- and chloro-bromo- complexes dominate (Fig. 5B). The peak currents for 5 nM Hg(II) measured with the AuNF-GIME and AuNP-GIME in 0.5M NaCl and UV-seawater sample were similar (Table 1) suggesting that the mixed Hg(II) chloro-bromo-complexes are also dynamic and therefore electrochemically accessible.

Adding the presence of natural hydrophilic low MW fulvic acid in vMINTEQ, the model predicts that all the added Hg(II) will be complexed with the strong DOM thiol and other sulfur-containing groups for DOM concentrations ≥ 0.6 mg/L (Fig. 5B). Despite this, no significant decrease in the Hg peak current (i.e. $\Delta i/\Delta i_{max}$ ratios ≥ 90%; where Δi and Δi_{max} is the subtractive SWASV currents recorded in presence and absence of fulvic acid respectively) were observed for the Au-GIME for increasing concentrations of fulvic acid (SRFA) up to 6 mg/L in the UV irradiated seawater sample (Fig. 5D). These results reflect that the Hg-SRFA are sufficient mobile to diffuse through the gel and sufficiently labile to contribute to $Hg(II)_{dyn}$ recorded with the nanostructured Au-GIME. The mobility of the Hg-SRFA is consistent with the SFRA diffusing properties in the agarose gel reported by Lead et al.[65] The lability of the Hg-SRFA suggests Hg(II) complexation with the abundant weak functional groups in DOM (*e.g.* carboxylic acids, phenols and other oxygen-containing functional groups). This might be explained by saturation of the strong sulfhydryl binding sites of DOM present at low concentration (~0.05 nM per 1 mg/L of DOM)[67] by other trace metals, especially Fe and Al that are present in concentration 10 to 1000 times higher that Hg and have stability constants similar to most of those reported for Hg for sulfhydryl binding sites.[68,69] Of course more detailed studies are needed to evaluate this hypothesis.

The $\Delta i/\Delta i_{max}$ ratios ≥ 90% also suggest that (i) the diffusing Hg-SRFA complexes have similar diffusion coefficients than Hg(II), and (ii) the SRFA diffusing through the gel does not sorb on the gold microdisk electrodes and therefore does not hamper the SWASV Hg(II) signals. Point (i) is a pre-requisite condition to allow for the quantification of $Hg(II)_{dyn}$ using external calibration with only free mercury in the presence of ≥ 0.2M Cl^-. According to the SRFA diffusion coefficient determined by flow field-flow fractionation[70] and the SRFA diffusing properties in 1.5% LGL agarose gel,[65] one may estimate the diffusion coefficient of SFRA in the gel as ~ 3.9×10^{-6} cm^2 s^{-1}. This value is comparable to the Hg(II) diffusion coefficients determined in section "Kinetics of Hg(II) diffusion

through the agarose gel" and thus supports a similar mobility of the small Hg(II) chloro- and SRFA complexes in the gel.

Field application and evaluation

In situ operation of the sensors was demonstrated during a 24 h deployment at the Comprian site in the Arcachon Bay conducted May 15th-16th, 2017. *In situ* autonomous hourly measurements of the dynamic concentration of Hg(II) dynamic species ($Hg(II)_{dyn}$) were performed with a 10x19-AuNF-GIME incorporated in a compact submersible multi-channel trace metal sensing probe (TracMetal).[15] Complementary measurements of total dissolved Hg(II) ($Hg(II)_{diss}$) by GC-ICP-MS and DOC were performed in samples collected at a 2 to 4h interval.

The temporal profiles of $Hg(II)_{dyn}$ and $Hg(II)_{diss}$ are presented in Fig.6 C. $Hg(II)_{dyn}$ and $Hg(II)_{diss}$ concentrations were similar, ranging respectively from 3.4 to 12.5 pM and 4.1 to 14.1 pM. These results suggest that inorganic Hg(II) at the Comprian site of the Arcachon Bay is mainly present in the dynamic form (see below). In addition, the good agreement between the Hg(II) concentrations measured with the two independent analytical techniques greatly supports the reliability and accuracy of the AuNF-GIME for the direct *in situ* detection of $Hg(II)_{dyn}$ at pM level. More specifically, it reflects the validity of the factor for temperature effect correction determined in laboratory for the first time (section "Temperature effect correction") and supports that the co-deposited Cu multilayers (see sub-section "Reliability and sensitivity of the Au-GIME") have a negligible influence on the electrochemical Hg(II) pre-concentration. If Cu at a much higher concentration were found to interfere with the Hg detection, a more positive potential should be used during the electrochemical preconcentration step to decrease the apparent Cu peak.[27] Another alternative would be to add intermittent short anodic pulses during the preconcentration step to strip most of the co-deposited Cu while Hg remains deposited, as demonstrated by Sipos et al.[23] The similar results obtained for the two independent analytical techniques, coupled to the similar normalized slopes obtained for the external and internal calibrations before and after deployment (see sub-section 2.4) also support similar diffusion coefficients for Hg(II) and the labile Hg(II)-organic complexes diffusing through the gel.

Interesting environmental information on $Hg(II)_{dyn}$ cycling could be obtained from the unique set of mercury and master variable data recorded *in situ* and at high-resolution during the 24 h cycle. The

temporal variation in salinity (Fig. 2A), ranging from 28.5 to 33.5, reflected the flux of fresh and marine waters at the site resulting from the semi-diurnal tide conditions. DOC (1.2 to 2 mg/L) and turbidity (2.3 to 10.5 NTU) were counter-cyclical to the diurnal variation in salinity (Figs. 6A, 6B). The maximum DOC concentrations and highest turbidity occurred at low tide suggesting an input of allochthonous DOC (*e.g.* fulvic and humic acids) and suspended particles carried out by the River Leyre and the other freshwater effluents. Interestingly, turbidity peaked-up at the early flood tide and late ebb tide reflecting a resuspension of sediment fluid-mud layers when the water flow rates were high.

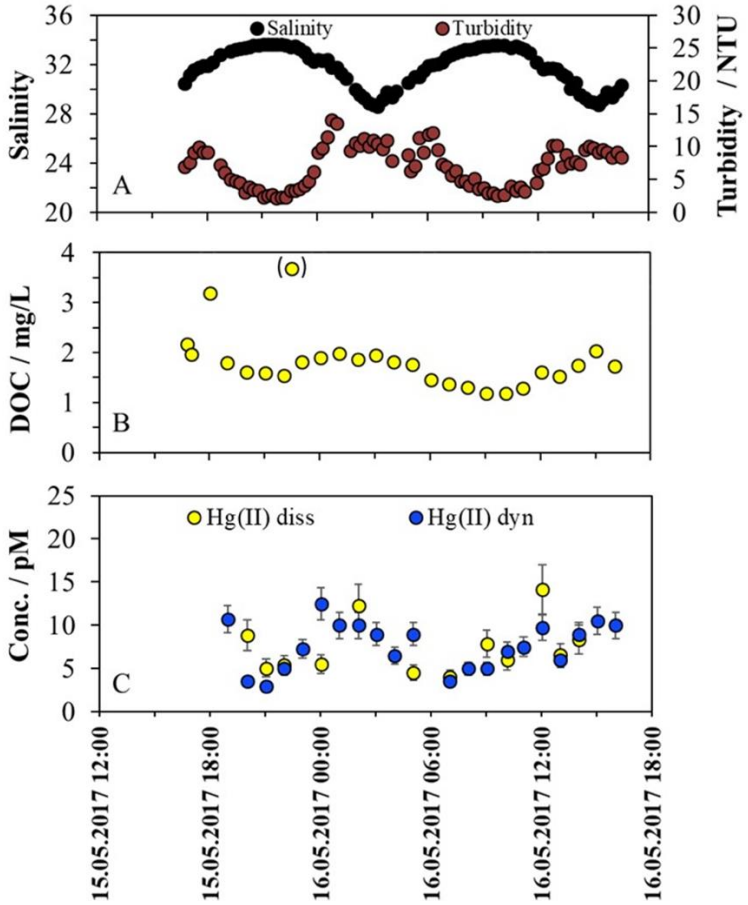

Figure 6: Temporal profiles of: (A) salinity and turbidity monitored *in situ* (multiparameter probe); (B) dissolved organic carbon (DOC; TOC analyzer); and (C) $Hg(II)_{dyn}$ monitored *in situ* by SWASV on a 10x19-AuNF-GIME and $Hg(II)_{diss}$ measured by GC-ICP-MS.

$Hg(II)_{dyn}$ temporal trend reflected also a tidal dependence with increasing and decreasing flux during respectively ebb tide and flow tide (Fig. 6 C). $Hg(II)_{dyn}$ was positively correlated (Pearson's

correlation coefficients r = 0.65, P < 0.01) with the concentration of the dissolved organic carbon (DOC). These later two findings are consistent with the outcome of previous studies showing that DOM acts as a vector of Hg in the land-ocean aquatic continuum.[71,72] The similar $Hg(II)_{dyn}$ and $Hg(II)_{diss}$ concentrations monitored suggest that the Hg-DOM complexes present at the Comprian site are mainly under a dynamic form, i.e. sufficiently labile and mobile to be detected by the AuNF-GIME interrogated by SWASV, and therefore potentially bioavailable. These results support the processes discussed in section "Evaluation of the dynamic Hg(II) species". Namely, the mobility of the Hg-DOM complexes is consistent with DOM in coastal water dominated by low molecular weight hydrophilic fulvic acid. The lability of the Hg-DOM complexes is consistent with Hg(II) binding to the DOM weak functional groups, that might be explained by the saturation of sulfhydryl strong binding sites by other metals. Moreover, it was observed that $Hg(II)_{dyn}$ peaked-up together with turbidity at the early flood tide and late ebb tide, i.e. at occurrence of tidal mudflats. These results suggest that tide-related resuspension processes may contribute to the release of $Hg(II)_{dyn}$ from the sediment into the water column, which might increases the risk of Hg exposure to estuarine ecosystems. They also illustrated the significant influence that "internal" processes may have on the $Hg(II)_{dyn}$ biogeochemical cycle, and therefore on the environmental and socioeconomic impact of Hg even long after its release has been reduced.

Conclusion

The development of reproducible and renewable nanostructured Au-plated GIMEs with the ability to directly quantify the dynamic (potentially bioavailable) fraction of inorganic mercury ($Hg(II)_{dyn}$) in marine aquatic systems has been successfully achieved. We showed for the first time that inorganic Hg at the low pM level can be monitored in seawater at natural pH by SWASV on gold electrode without medium exchange; sample filtration, UV irradiation, and acidification; nor chemical electrode surface modification. This was achieved by combining several innovative analytical approaches. Detection limits were lowered by optimizing the number of interconnected microelectrodes, the surface of the chip, the morphology of the gold-nanostructured sensing surface, and to increase the pre-concentration time up to 30 min, if required. The oxidation of gold to gold-halide complexes was minimized by working at natural pH, adding a halide desorption step in the SWASV measurement protocol and optimising the final potential of the stripping ramp. Fouling of

the sensors by suspended inorganic matters and dissolved organic compounds was minimized by covering the sensor surface with an agarose gel acting as an efficient antifouling membrane. These developments are generic and may be considered for the field monitoring of other metals, *e.g.* inorganic arsenite,[35] and potentially arsenate[61] and copper (see section "Reliability and sensitivity of the Au-GIME"). Field application of the AuNF-GIME placed in an in-house compact multichannel submersible trace metal sensing probe (TracMetal) for direct quantification of $Hg(II)_{dyn}$ was successfully achieved. The accuracy of the high-resolution (1 measurements h^{-1}) $Hg(II)_{dyn}$ concentrations monitored *in situ* in autonomous mode was demonstrated by intercomparison with laboratory GC-ICP-MS measurements performed in collected samples. The field data demonstrated the capability of this unique sensor probe to track in near real-time small variation of $Hg(II)_{dyn}$ in highly dynamic coastal area and, when coupled to a commercial multiparameter probe for the measurements of master bio-physicochemical parameters, to assess "external" and "internal" processes that influence the geochemical cycle of potentially bioavailable Hg(II), The AuNF-GIME TracMetal system is therefore a promising tool that may serve as efficient sentinel and alarm system into spatial and temporal environmental monitoring programs for mercury ecological and socio-economic risk assessment.

Acknowledgements

We thank the European Union (FP7 Ocean 2013.2 - Project SCHeMA, Grant Agreement 614002) for the financial support of this research. The authors also gratefully acknowledge the help of the R/V Planula IV Crew (TGIR FOF), Dr Lionel Dutruch for support in GC- ICP-MS measurements, and Dr Sandrine Mongin for running the vMINTEQ simulation.

References

(1) Obrist, D.; Kirk, J. L.; Zhang, L.; Sunderland, E. M.; Jiskra, M.; Selin, N. E. A Review of Global Environmental Mercury Processes in Response to Human and Natural Perturbations: Changes of Emissions, Climate, and Land Use. *Ambio* **2018**, *47* (2), 116–140. https://doi.org/10.1007/s13280-017-1004-9.

(2) Lavoie, R. A.; Jardine, T. D.; Chumchal, M. M.; Kidd, K. A.; Campbell, L. M. Biomagnification of Mercury in Aquatic Food Webs: A Worldwide Meta-Analysis. *Environmental Science & Technology* **2013**, *47*, 13385–13394. https://doi.org/10.1021/es403103t.

(3) Le Faucheur, S.; Campbell, P. G. C.; Fortin, C.; Slaveykova, V. I. Interactions between Mercury and Phytoplankton: Speciation, Bioavailability, and Internal Handling: Mercury-Phytoplankton Interactions. *Environ Toxicol Chem* **2014**, *33* (6), 1211–1224. https://doi.org/10.1002/etc.2424.

(4) Beauvais-Flück, R.; Slaveykova, V.; Cosio, C. Molecular Effects of Inorganic and Methyl Mercury in Aquatic Primary Producers: Comparing Impact to A Macrophyte and A Green Microalga in Controlled Conditions. *Geosciences* **2018**, *8* (11), 393. https://doi.org/10.3390/geosciences8110393.

(5) UN Environment. Global Mercury Assessment 2018. UN Environment Programme, Chemicals and Health Branch Geneva, Switzerland. **2019**. https://wedocs.unep.org/bitstream/handle/20.500.11822/27579/GMA2018.pdf.

(6) *Global and Regional Mercury Cycles: Sources, Fluxes and Mass Balances*; Baeyens, W., Ebinghaus, R., Vasiliev, O., Eds.; Springer Netherlands: Dordrecht, 1996. https://doi.org/10.1007/978-94-009-1780-4.

(7) AMAP. AMAP Assessment 2011: Mercury in the Arctic. Arctic Monitoring and Assessment Programme (AMAP), Oslo, Norway. **2011**. https://www.amap.no/documents/doc/amap-assessment-2011-mercury-in-the-arctic/90.

(8) Streets, D. G.; Zhang, Q.; Wu, Y. Projections of Global Mercury Emissions in 2050. *Environ. Sci. Technol.* **2009**, *43* (8), 2983–2988. https://doi.org/10.1021/es802474j.

(9) AMAP/UN Environment. Technical Background Report for the Global Mercury Assessment 2018. Arctic Monitoring and Assessment Programme, Oslo, Norway/UN Environment Programme, Chemicals and Health Branch, Geneva, Switzerland. 2019.

(10) Lamborg, C. H.; Hammerschmidt, C. R.; Bowman, K. L.; Swarr, G. J.; Munson, K. M.; Ohnemus, D. C.; Lam, P. J.; Heimbürger, L.-E.; Rijkenberg, M. J. A.; Saito, M. A. A Global Ocean Inventory of Anthropogenic Mercury Based on Water Column Measurements. *Nature* **2014**, *512* (7512), 65–68. https://doi.org/10.1038/nature13563.

(11) Zhang, Y.; Jaeglé, L.; Thompson, L.; Streets, D. G. Six Centuries of Changing Oceanic Mercury: Anthropogenic Mercury in Ocean. *Global Biogeochem. Cycles* **2014**, *28* (11), 1251–1261. https://doi.org/10.1002/2014GB004939.

(12) Wang, F.; Zhang, J. Mercury Contamination in Aquatic Ecosystems under a Changing Environment: Implications for the Three Gorges Reservoir. *Chin. Sci. Bull.* **2013**, *58* (2), 141–149. https://doi.org/10.1007/s11434-012-5490-7.

(13) Fitzgerald, W. F.; Lamborg, C. H.; Hammerschmidt, C. R. Marine Biogeochemical Cycling of Mercury. *Chem. Rev.* **2007**, *107* (2), 641–662. https://doi.org/10.1021/cr050353m.

(14) Mason, R. P.; Gill, G. A. Mercury in the Marine Environment, Chap. 10. In *Mercury Sources, Measurements, Cycles, and Effects*; Mineralogical Association of Canada. Short Course Series; Nova Scotia, Canada: Halifax, 2005; Vol. 34, pp 179–216.
(15) Tercier-Waeber, M.-L.; Confalonieri, F.; Abdou, M.; Dutruch, L.; Bossy, C.; Fighera, M.; Bakker, E.; Graziottin, F.; van der Wal, P.; Schäfer, J. Advanced multichannel submersible probe for autonomous high-resolution in situ measurements of the cycling of the potentially bioavailable fraction of a range of trace metals. *Environ. Sci. Technol., submitted* **2021**.
(16) Tercier-Waeber, M.-L.; Taillefert, M. Remote in Situ Voltammetric Techniques to Characterize the Biogeochemical Cycling of Trace Metals in Aquatic Systems. *J. Environ. Monit.* **2008**, *10* (1), 30–54. https://doi.org/10.1039/B714439N.
(17) Andrews, R. W.; Larochelle, J. H.; Johnson, D. C. Determination of Trace Mercury(II) in 0.1 M Perchloric Acid by Differential Pulse Stripping Voltammetry at a Rotating Gold Disc Electrode. *Anal. Chem.* **1976**, *48* (1), 212–214. https://doi.org/10.1021/ac60365a025.
(18) Herrero, E.; Abruña, H. D. Underpotential Deposition of Mercury on Au(111): Electrochemical Studies and Comparison with Structural Investigations. *Langmuir* **1997**, *13* (16), 4446–4453. https://doi.org/10.1021/la970109t.
(19) Li, J.; Herrero, E.; Abruña, H. D. The Effects of Anions on the Underpotential Deposition of Hg on Au(111) An Electrochemical and in Situ Surface X-Ray Diffraction Study. *Colloids and Surfaces A: Physicochemical and Engineering Aspects* **1998**, *134* (1–2), 113–131. https://doi.org/10.1016/S0927-7757(97)00341-5.
(20) Salié, G.; Bartels, K. Partial Charge Transfer in the Underpotential Deposition of Metals. *Journal of Electroanalytical Chemistry and Interfacial Electrochemistry* **1988**, *245* (1–2), 21–38. https://doi.org/10.1016/0022-0728(88)80056-1.
(21) Bonfil, Y.; Brand, M.; Kirowa-Eisner, E. Trace Determination of Mercury by Anodic Stripping Voltammetry at the Rotating Gold Electrode. *Analytica Chimica Acta* **2000**, *424* (1), 65–76. https://doi.org/10.1016/S0003-2670(00)01074-6.
(22) Gustavsson, I. Determination of Mercury in Sea Water by Stripping Voltammetry. *Journal of Electroanalytical Chemistry and Interfacial Electrochemistry* **1986**, *214* (1–2), 31–36. https://doi.org/10.1016/0022-0728(86)80083-3.
(23) Sipos, L.; Nürnberg, H. W.; Valenta, P.; Branica, M. The Reliable Determination of Mercury Traces in Sea Water by Subtractive Differential Pulse Voltammetry at the Twin Gold Electrode. *Analytica Chimica Acta* **1980**, *115*, 25–42. https://doi.org/10.1016/S0003-2670(01)93140-X.
(24) Khustenko, L. A.; Larina, L. N.; Nazarov, B. F. Rapid Determination of Mercury in Water by Stripping Voltammetry at a Gold-Modified Carbon Electrode. *Journal of Analytical Chemistry* **2003**, *58* (3), 262–267. https://doi.org/10.1023/A:1022694606107.
(25) Sanchez, J.; Castillo, E.; Corredor, P.; Ágreda, J. Determination of Mercury by Anodic Stripping Voltammetry in Aqua Regia Extracts: *Port. Electrochim. Acta* **2011**, *29* (3), 197–210. https://doi.org/10.4152/pea.201103197.
(26) Daniele, S.; Bragato, C.; Antonietta Baldo, M.; Wang, J.; Lu, J. The Use of a Remote Stripping Sensor for the Determination of Copper and Mercury in the Lagoon of Venice. *Analyst* **2000**, *125* (4), 731–735. https://doi.org/10.1039/a908540h.
(27) Salaün, P.; van den Berg, C. M. G. Voltammetric Detection of Mercury and Copper in Seawater Using a Gold Microwire Electrode. *Analytical Chemistry* **2006**, *78*, 5052–5060. https://doi.org/10.1021/ac060231+.

(28) Garnier, C.; Lesven, L.; Billon, G.; Magnier, A.; Mikkelsen, Ø.; Pižeta, I. Voltammetric Procedure for Trace Metal Analysis in Polluted Natural Waters Using Homemade Bare Gold-Disk Microelectrodes. *Anal Bioanal Chem* **2006**, *386* (2), 313–323. https://doi.org/10.1007/s00216-006-0625-9.
(29) Ordeig, O.; Banks, C. E.; del Campo, J.; Muñoz, F. X.; Compton, R. G. Trace Detection of Mercury(II) Using Gold Ultra-Microelectrode Arrays. *Electroanalysis* **2006**, *18* (6), 573–578. https://doi.org/10.1002/elan.200503437.
(30) Laffont, L.; Hezard, T.; Gros, P.; Heimbürger, L.-E.; Sonke, J. E.; Behra, P.; Evrard, D. Mercury(II) Trace Detection by a Gold Nanoparticle-Modified Glassy Carbon Electrode Using Square-Wave Anodic Stripping Voltammetry Including a Chloride Desorption Step. *Talanta* **2015**, *141*, 26–32. https://doi.org/10.1016/j.talanta.2015.03.036.
(31) Hay, C. E.; Lee, J.; Silvester, D. S. Formation of 3-Dimensional Gold, Copper and Palladium Microelectrode Arrays for Enhanced Electrochemical Sensing Applications. *Nanomaterials* **2019**, *9* (8), 1170. https://doi.org/10.3390/nano9081170.
(32) Podešva, P.; Gablech, I.; Neužil, P. Nanostructured Gold Microelectrode Array for Ultrasensitive Detection of Heavy Metal Contamination. *Anal. Chem.* **2018**, *90* (2), 1161–1167. https://doi.org/10.1021/acs.analchem.7b03725.
(33) Said, N. A. M.; Ogurtsov, V. I.; Twomey, K.; Nagle, L. C.; Herzog, G. Chemically Modified Electrodes for Recessed Microelectrode Array. *Procedia Chemistry* **2016**, *20*, 12–24. https://doi.org/10.1016/j.proche.2016.07.002.
(34) Touilloux, R.; Tercier-Waeber, M.-L.; Bakker, E. Antifouling Membrane Integrated Renewable Gold Microelectrode for in Situ Detection of As(III). *Anal. Methods* **2015**, *7* (18), 7503–7510. https://doi.org/10.1039/C5AY01941A.
(35) Tercier-Waeber, M.-L.; Fighera, M.; Abdou, M.; Bakker, E.; van der Wal, P. Newly Designed Gel Integrated Nanostructured Gold-Based Interconnected Microelectrode Arrays for Direct Arsenite Monitoring in Aquatic Systems. *Sensors and Actuators B* **2021**, https://doi.org/10.1016/j.snb.2020.128996.
(36) Buffle, J.; Tercier-Waeber, M.-L. Voltammetric Environmental Trace-Metal Analysis and Speciation: From Laboratory to in Situ Measurements. *TrAC Trends in Analytical Chemistry* **2005**, *24* (3), 172–191. https://doi.org/10.1016/j.trac.2004.11.013.
(37) Buffle, J.; Tercier-Waeber, M.-L. In Situ Voltammetry: Concepts and Practice for Trace Analysis and Speciation, Chap 9. In *In situ monitoring of aquatic systems; Chemical analysis and speciation*; IUPAC Series; Wiley: Chichester, 2000; Vol. 6, pp 279–405.
(38) *Microelectrodes: Theory and Applications*; Montenegro, I. M., Queirós, M. A., Daschbach, J. L., Eds.; Springer Netherlands: Dordrecht, 1991. https://doi.org/10.1007/978-94-011-3210-7.
(39) Pletcher, D. Why Microelectrodes? In *Microelectrodes: Theory and Applications*; Montenegro, M. I., Queirós, M. A., Daschbach, J. L., Eds.; Springer Netherlands: Dordrecht, 1991; pp 3–16. https://doi.org/10.1007/978-94-011-3210-7_1.
(40) Belmont-Hébert, C.; Tercier, M. L.; Buffle, J.; Fiaccabrino, G. C.; de Rooij, N. F.; Koudelka-Hep, M. Gel-Integrated Microelectrode Arrays for Direct Voltammetric Measurements of Heavy Metals in Natural Waters and Other Complex Media. *Anal. Chem.* **1998**, *70* (14), 2949–2956. https://doi.org/10.1021/ac971194c.
(41) Tercier, M.-L.; Buffle, J. Antifouling Membrane-Covered Voltammetric Microsensor for in Situ Measurements in Natural Waters. *Anal. Chem.* **1996**, *68* (20), 3670–3678. https://doi.org/10.1021/ac960265p.

(42) Fatin-Rouge, N.; Starchev, K.; Buffle, J. Size Effects on Diffusion Processes within Agarose Gels. *Biophysical Journal* **2004**, *86* (5), 2710–2719. https://doi.org/10.1016/S0006-3495(04)74325-8.
(43) Sigg, L.; Black, F.; Buffle, J.; Cao, J.; Cleven, R.; Davison, W.; Galceran, J.; Gunkel, P.; Kalis, E.; Kistler, D.; Martin, M.; Noël, S.; Nur, Y.; Odzak, N.; Puy, J.; van Riemsdijk, W.; Temminghoff, E.; Tercier-Waeber, M.-L.; Toepperwien, S.; Town, R. M.; Unsworth, E.; Warnken, K. W.; Weng, L.; Xue, H.; Zhang, H. Comparison of Analytical Techniques for Dynamic Trace Metal Speciation in Natural Freshwaters. *Environ. Sci. Technol.* **2006**, *40* (6), 1934–1941. https://doi.org/10.1021/es051245k.
(44) van Leeuwen, H. P.; Town, R. M.; Buffle, J.; Cleven, R. F. M. J.; Davison, W.; Puy, J.; van Riemsdijk, W. H.; Sigg, L. Dynamic Speciation Analysis and Bioavailability of Metals in Aquatic Systems. *Environ. Sci. Technol.* **2005**, *39* (22), 8545–8556. https://doi.org/10.1021/es050404x.
(45) Buffle, J.; Wilkinson, K. J.; van Leeuwen*, H. P. Chemodynamics and Bioavailability in Natural Waters. *Environ. Sci. Technol.* **2009**, *43* (19), 7170–7174. https://doi.org/10.1021/es9013695.
(46) Tercier-Waeber, M.-L.; Stoll, S.; Slaveykova, V. Trace Metal Behavior in Surface Waters: Emphasis on Dynamic Speciation, Sorption Processes and Bioavailability. *Archives des Sciences* **2012**, *65*, 119–142.
(47) Tercier, M.-L.; Buffle, J.; Graziottin, F. A Novel Voltammetric In-Situ Profiling System for Continuous Real-Time Monitoring of Trace Elements in Natural Waters. *Electroanalysis* **1998**, *10*, 355–363. https://doi.org/10.1002/(SICI)1521-4109(199805)10:6<355::AID-ELAN355>3.0.CO;2-F.
(48) Komsiyska, L.; Staikov, G. Electrocrystallization of Au Nanoparticles on Glassy Carbon from HClO4 Solution Containing [AuCl4]−. *Electrochimica Acta* **2008**, *54* (2), 168–172. https://doi.org/10.1016/j.electacta.2008.08.013.
(49) Tercier-Waeber, M.-L.; Buffle, J. Submersible Online Oxygen Removal System Coupled to an in Situ Voltammetric Probe for Trace Element Monitoring in Freshwater. *Environ. Sci. Technol.* **2000**, *34* (18), 4018–4024. https://doi.org/10.1021/es000033e.
(50) Monperrus, M.; Krupp, E.; Amouroux, D.; Donard, O. F. X.; Rodríguez Martín-Doimeadios, R. C. Potential and Limits of Speciated Isotope-Dilution Analysis for Metrology and Assessing Environmental Reactivity. *TrAC Trends in Analytical Chemistry* **2004**, *23* (3), 261–272. https://doi.org/10.1016/S0165-9936(04)00313-9.
(51) Sharp, J. H.; Benner, R.; Bennett, L.; Carlson, C. A.; Dow, R.; Fitzwater, S. E. Re-Evaluation of High Temperature Combustion and Chemical Oxidation Measurements of Dissolved Organic Carbon in Seawater. *Limnol. Oceanogr.* **1993**, *38* (8), 1774–1782. https://doi.org/10.4319/lo.1993.38.8.1774.
(52) Moretto, L. M.; Mazzocchin, G. A.; Ugo, P. Electroanalytical Study on the Ion-Exchange Voltammetric Behaviour of Hg(II) at Tosflex®-Coated Glassy Carbon Electrodes. *Journal of Electroanalytical Chemistry* **1997**, *427* (1–2), 113–121. https://doi.org/10.1016/S0022-0728(96)05004-8.
(53) Belevantsev, V. I.; Malkova, V. I.; Gushchina, L. V.; Obolenskii, A. A. Chloro Complexes of Mercury(II) in Aqueous Perchlorate Media: Equilibrium and Electronic Absorption Spectra. *Russian Journal of Coordination Chemistry* **2004**, *30* (7), 465–472. https://doi.org/10.1023/B:RUCO.0000034786.68915.69.
(54) Jost, W. *Diffusion in Solids, Liquids, Gases*, Academic Press.; New-York, 1951.

(55) Henry, V. K. *CRC Handbook of Thermophysical and Thermochemical Data*, CRC Press Inc.; Boca Raton, 1994.
(56) Tercier-Waeber, M.-L.; Confalonieri, F.; Koudelka-Hep, M.; Dessureault-Rompré, J.; Graziottin, F.; Buffle, J. Gel-Integrated Voltammetric Microsensors and Submersible Probes as Reliable Tools for Environmental Trace Metal Analysis and Speciation. *Electroanalysis* **2008**, *20* (3), 240–258. https://doi.org/10.1002/elan.200704067.
(57) Tercier-Waeber, M.-L.; Buffle, J.; Confalonieri, F.; Riccardi, G.; Sina, A.; Graziottin, F.; Fiaccabrino, G. C.; Koudelka-Hep, M. Submersible Voltammetric Probes for in Situ Real-Time Trace Element Measurements in Surface Water, Groundwater and Sediment-Water Interface. *Meas. Sci. Technol.* **1999**, *10* (12), 1202–1213. https://doi.org/10.1088/0957-0233/10/12/312.
(58) Pei, J.; Tercier-Waeber, M.-L.; Buffle, J. Simultaneous Determination and Speciation of Zinc, Cadmium, Lead, and Copper in Natural Water with Minimum Handling and Artifacts, by Voltammetry on a Gel-Integrated Microelectrode Array. *Anal. Chem.* **2000**, *72* (1), 161–171. https://doi.org/10.1021/ac990628w.
(59) Tercier-Waeber, M.-L.; Hezard, T.; Masson, M.; Schäfer, J. In Situ Monitoring of the Diurnal Cycling of Dynamic Metal Species in a Stream under Contrasting Photobenthic Biofilm Activity and Hydrological Conditions. *Environ. Sci. Technol.* **2009**, *43* (19), 7237–7244. https://doi.org/10.1021/es900247y.
(60) Tercier-Waeber, M.-L.; Belmont-Hébert, C.; Buffle, J. Real-Time Continuous Mn(II) Monitoring in Lakes Using a Novel Voltammetric in Situ Profiling System. *Environ. Sci. Technol.* **1998**, *32* (10), 1515–1521. https://doi.org/10.1021/es9706108.
(61) Penezić, A.; Tercier-Waeber, M.-L.; Abdou, M.; Bossy, C.; Dutruch, L.; Bakker, E.; Schäfer, J. Spatial Variability of Arsenic Speciation in the Gironde Estuary: Emphasis on Dynamic (Potentially Bioavailable) Inorganic Arsenite and Arsenate Fractions. *Marine Chemistry* **2020**, *223*, 103804. https://doi.org/10.1016/j.marchem.2020.103804.
(62) Penru, Y.; Simon, F. X.; Guastalli, A. R.; Esplugas, S.; Llorens, J.; Baig, S. Characterization of Natural Organic Matter from Mediterranean Coastal Seawater. *Journal of Water Supply: Research and Technology-Aqua* **2013**, *62* (1), 42–51. https://doi.org/10.2166/aqua.2013.113.
(63) Shimotori, K.; Satou, T.; Imai, A.; Kawasaki, N.; Komatsu, K.; Kohzu, A.; Tomioka, N.; Shinohara, R.; Miura, S. Quantification and Characterization of Coastal Dissolved Organic Matter by High-Performance Size Exclusion Chromatography with Ultraviolet Absorption, Fluorescence, and Total Organic Carbon Analyses: Size and Characterization of Coastal DOM. *Limnol. Oceanogr. Methods* **2016**, *14* (10), 637–648. https://doi.org/10.1002/lom3.10118.
(64) Lead, J. R.; Wilkinson, K. J.; Balnois, E.; Cutak, B. J.; Larive, C. K.; Assemi, S.; Beckett, R. Diffusion Coefficients and Polydispersities of the Suwannee River Fulvic Acid: Comparison of Fluorescence Correlation Spectroscopy, Pulsed-Field Gradient Nuclear Magnetic Resonance, and Flow Field-Flow Fractionation. *Environ. Sci. Technol.* **2000**, *34* (16), 3508–3513. https://doi.org/10.1021/es991195h.
(65) Lead, J. R.; Starchev, K.; Wilkinson, K. J. Diffusion Coefficients of Humic Substances in Agarose Gel and in Water. *Environ. Sci. Technol.* **2003**, *37* (3), 482–487. https://doi.org/10.1021/es025840n.
(66) Lindgren, B.; Jonsson, A.; Sillén, L. G.; Linnasalmi, A.; Laukkanen, P. Electrometric Investigation of Equilibria between Mercury and Halogen Ions.V. Complexes between Hg2+ and Cl-. *Acta Chem. Scand.* **1947**, *1*, 479–488. https://doi.org/10.3891/acta.chem.scand.01-0479.

(67) Loux, N. T. An Assessment of Mercury-Species-Dependent Binding with Natural Organic Carbon. *Chemical Speciation & Bioavailability* **1998**, *10* (4), 127–136. https://doi.org/10.3184/095422998782775754.
(68) Yang, R.; van den Berg, C.M.G. Metal complexation by humic substnces in seawater. *Environ. Sci. Technol.* **2009**, *43*, 7192-7197. https://doi.org/10.1021/es900173w
(69) Ravichandran, M. Interactions between mercury and dissolved organic matter – a review. Chemosphere **2004**, *55*, 319-331. https://doi.org/10.1016/j.chemosphere.2003.11.011
(70) Beckett, Ronald.; Jue, Zhang.; Giddings, J. Calvin. Determination of Molecular Weight Distributions of Fulvic and Humic Acids Using Flow Field-Flow Fractionation. *Environ. Sci. Technol.* **1987**, *21* (3), 289–295. https://doi.org/10.1021/es00157a010.
(71) Bi, C.; Chen, Z.; Shen, J.; Sun, W. Variations of Mercury Distribution in the Water Column during the Course of a Tidal Cycle in the Yangtze Estuarine Intertidal Zone, China. *Sci. China Chem.* **2012**, *55* (10), 2224–2232. https://doi.org/10.1007/s11426-012-4622-x.
(72) Cesário, R.; Mota, A. M.; Caetano, M.; Nogueira, M.; Canário, J. Mercury and Methylmercury Transport and Fate in the Water Column of Tagus Estuary (Portugal). *Marine Pollution Bulletin* **2018**, *127*, 235–250. https://doi.org/10.1016/j.marpolbul.2017.11.066.

For TOC only

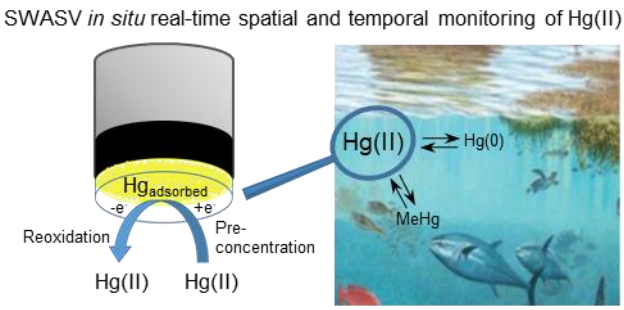
SWASV *in situ* real-time spatial and temporal monitoring of Hg(II)
Hg adsorbed
-e
+e
Reoxidation
Pre-concentration
Hg(II)
Hg(II)
Hg(II)
Hg(0)
MeHg